Self-calibration of geometric and radiometric parameters for cone-beam computed tomography

Wolfgang Wein, Alexander Ladikos and Armin Baumgartner

***Abstract*—Thanks to the advances in parallel processing hardware, iterative algorithms for cone beam reconstruction are now available with computation times acceptable for clinical use. At the same time they are able to accomodate more accurately the physical effects underlying the X-Ray imaging process. Many parameters are involved, which need to be precisely calibrated in order to achieve an accurate 3D reconstruction. Unfortunately, some parameters might change individually for every cone beam acquisition, stirring the need for an online calibration technique. We present a method for automatically deriving individual parameter adjustements within an iterative reconstruction framework, without the need for a designated calibration phantom. Preliminary results on a beads phantom and anatomical sample show that self-calibration of global and local geometric parameters is possible; besides we briefly demonstrate radiometric calibration on phantom data.**

***Index Terms*—cone-beam, computed tomography, reconstruction, OS-SIRT, calibration.**

I. Introduction

Cone-beam reconstruction algorithms comprise an essential technology in all 3D X-Ray based image modalities. Expensive clinical computed tomography (CT) scanners nowadays use 3D cone-beam rather than 2D fan-beam reconstruction methods due to the trend to many-slice systems. Recent advances in flat-panel detector technology also spawns small cone-beam tomography systems with unprecedented image quality. Those digital volume tomography (DVT) devices are mainly used in ENT and dental applications, providing excellent reconstructions within a small volume, for a price an order of magnitude smaller than CT systems. This typically low price tag however limits the mechanical accuracy of the rotational movement as well as precise per-unit calibration of all X-Ray source, detector, and geometric parameters. The trend to powerful iterative reconstruction techniques, resulting in a more complete modeling of X-Ray physics, also raises the requirement of correctly estimating more, especially radiometric, parameters. It is therefore desirable that the arising unknowns be recovered automatically in the reconstruction software, in particular since some of them might change during every individual acquisition.

Offline calibration of cone-beam systems is a problem that has been well understood and solved by every manufacturer, with a variety of calibration phantoms and algorithms available. Online computation of the individual projection parameters of a cone-beam run has been developed as well. Such methods either use additional sensors [1] or additional calibration markers that are placed around the patient [2]. Particularly the latter is nowadays prohibitive, since for DVT applications the reconstruction volume is fully covered by anatomy. Besides, modern radiation safety laws prohibit irradiating any body parts which are not used for image creation. An initial approach for re-calibration without additional information is shown in [3], using an optimization of global geometric parameters by entropy minimization of the volume in a FDK reconstruction.

In the following, we present our new method for automatically deriving geometric and radiometric parameters, both globally and for individual projections, within the reconstruction of the object to be diagnosed itself. It is based on an efficient simultaneous algebraic reconstruction, wherein the additional parameters are optimized. As opposed to [3] it optimizes the same criterion than the reconstruction itself and is generalized over any unknown parameters of the imaging device.

White Lion Technologies AG, Fürstenrieder Str. 275, 81377 München, Germany. Corresponding author: Wolfgang Wein, E-mail: wein@wlt.ag.

II. Methods

A. Reconstruction Framework

We have developed an efficient GPU implementation of an ordered subset simultaneous iterative reconstruction technique (OS-SIRT), similar to the one described in [4]. A subset of all X-Ray projection images is forward- and back-projected iteratively to yield the reconstructed volume. Let us introduce some variables:

- $V^{(k)}$ reconstruction volume estimate in iteration k
- N_V: number of voxels inside the reconstruction volume
- $v_j, j \in [1 \dots N_V]$: an individual voxel
- N_L: number of pixels in an X-Ray image
- $x_{il}, l \in \{1 \dots N_L\}$: a pixel of X-Ray image i
- r_{il}: single forward projected ray
- S_k: Frame indices of the subset used in iteration k
- $\mathbf{P}_i$: projection matrix of X-Ray image i
- $w_{jl}(\mathbf{P}_i)$: ray projection weights for image i
- $\lambda \in]0 \dots 1]$: relaxation factor

The forward projection operator is then written as

$$\forall i \in S_k, l \in \{1 \dots N_L\} : r_{il}^{(k)} = \sum_{j=1}^{N_V} v_j^{(k)} w_{jl}(\mathbf{P}_i) \quad (1)$$

The corresponding error back-propagation operator is

$$\forall j \in [1 \dots N_V] : v_j^{(k+1)} = v_j^{(k)} + \lambda \sum_{i \in S_k} \sum_{l=1}^{N_L} \frac{x_{il} - r_{il}^{(k)}}{\sum w_{jl}(\mathbf{P}_i)} \quad (2)$$

The ray projection weights $w_{jl}(\mathbf{P}_i)$ in both equations 1 and 2 are computed on the fly by the GPU, as texture interpolation weights along the rays.

B. Optimization Approach

In the framework described above, a single iteration k essentially tries to minimize the re-projection error E_k of subset S_k:

$$E_k = \sum_{i \in S_k} \sum_{l=1}^{N_L} \left| x_{il} - r_{il}^{(k)} \right| \tag{3}$$

In the ideal case, where the forward projection operator properly models the underlying X-Ray physics, this error should converge to zero after sufficient iterations. The idea is now to also minimize equation 3 with respect to all geometric parameters contained in $\mathbf{P}_i$ that are in question:

$$\hat{\mathbf{P}}_i = \arg\min_{\mathbf{P}_i} E_k \tag{4}$$

On top of that, further radiometric parameters, e.g. considering polychromaticity or scattering, might be included. The resulting list of parameters can unfortunately not be subject for iterative refinement within the OS-SIRT reconstruction, since successive iterations would create an inconsistent volume estimate while the parameters are changing. Rather, we have to create an outer optimization loop, repeatedly computing equation 3 after a complete reconstruction (i.e., all subsets have been used once). In this 'self-calibration' mode, we use down-sampled copies of the X-Ray images, yielding smaller values of N_V and N_L. Besides, if the subset size is large enough (typically $|S_k| \in [5 \dots 30]$ in our case), the value of E_k can be computed from the difference images of the last OS-SIRT subset execution. The problem then becomes computationally feasible, due to the capabilities of modern stream processing hardware.

Because of the iterative nature of the reconstruction itself, it is not directly possible to compute derivatives of E_k with regard to the parameters subject to optimization. For global geometric and radiometric parameters, we therefore use the Amoeba direct search method. Parameters which affect every individual frame i, can be successively optimized. The reconstruction is then repeated only after all projections have been adjusted.

C. Geometric Parameterization

For modeling the projection geometry we use a standard pinhole camera model [5]. The corresponding projection matrix $\mathbf{P}_i$ has dimensions 3×4 and can be decomposed into intrinsic and extrinsic camera parameters:

$$\mathbf{P}_i = \mathbf{K} \begin{bmatrix} \mathbf{R}_i & \mathbf{t} \end{bmatrix} = \begin{bmatrix} f_x & 0 & c_x \\ 0 & f_y & c_y \\ 0 & 0 & 1 \end{bmatrix} \begin{bmatrix} \mathbf{R} & \mathbf{t} \end{bmatrix} \tag{5}$$

where $\mathbf{K}$ is the intrinsic calibration matrix containing the focal lengths f_x and f_y in the respective axis directions and the principal point $(c_x, c_y)^\top$. $\mathbf{R}_i$ and $\mathbf{t}$ represent the extrinsic rotation and translation transforming the world coordinate system into the camera coordinate system.

During optimization, however, we do not directly optimize over this parametrization, but instead use a parametrization more suited to the source-detector geometry. The intrinisc calibration matrix can then be written as:

$$f_x = \frac{p_x}{s_x} d, \qquad f_y = \frac{p_y}{s_y} d \tag{6}$$

$$c_x = \frac{p_x}{2} + \frac{h_x}{s_x} p_x, \quad c_y = \frac{p_y}{2} + \frac{\tan(\alpha) d}{s_y} p_y \tag{7}$$

Here, d is the source-detector distance in mm, s_x and s_y is the size of the detector in mm and p_x and p_y are the dimensions of the projection image in pixels. h_x is the x-offset of the detector center from the intersection point of the X-ray source's principal ray in mm. α is the angle at which the detector is tilted with respect to the plane orthogonal to the X-ray source's principal ray ($\alpha \approx 6^\circ$ for dental applications, in order to avoid attenuating the same X-rays with teeth or implants on both sides).

The extrinsic camera parameters $\mathbf{R}_i$ and $\mathbf{t}$ are parameterized as:

$$\mathbf{R}_i = \begin{bmatrix} -\cos(\gamma_i) & -sin(\gamma_i) & 0 \\ 0 & 0 & 1 \\ -\sin(\gamma_i) & cos(\gamma_i) & 0 \end{bmatrix}, \quad \mathbf{t} = \begin{bmatrix} k_x \\ k_y \\ k_z \end{bmatrix} \tag{8}$$

where $\gamma_i = \frac{R}{N_X - 1}(o_i + i)$ with N_X the number of X-ray projections acquired, R the angle covered by the source-detector pair around the object and o_i the offset to the expected angle for frame i. This offset is necessary to accomodate slight mechanical variations in the angle increment when the device is moving. The vector (k_x, k_y, k_z) is the offset of the detector-source pair from the isocenter in mm. If k_x or k_y are non-zero the detector-source pair is describing an eccentric motion around the object instead of a circular one.

In this work, we chose to evaluate the optimization of o_i as an unknown parameter that is specific for every frame i. Please note that further parameters from $\mathbf{R}$ and $\mathbf{t}$ can be selected as frame-variant to achieve greater accuracy, depending on the mechanical setup.

D. Radiometric Parameterization

We have adapted the forward- and back-projection operators to incorporate a polychromatic X-Ray model, inspired by the work in [6]. This model tries to reconstruct linear attenuation cofficients at a selected energy, by approximately mapping them to photo-electric and compton cross-sections and calculating polychromatic line integrals. The modified forward projection operator is:

$$\forall i \in S_k, l \in \{1 \dots N_L\} : r_{il}^{(k)} = -\log \sum_{e=1}^{N_E} b_e \exp\left(\dots \right.$$
$$\left. -\Phi_e \sum_{j=1}^{N_V} \phi\left(v_j^{(k)}\right) w_{jl} - \Theta_e \sum_{j=1}^{N_V} \theta\left(v_j^{(k)}\right) w_{jl} \right) \tag{9}$$

where ϕ and θ are the mapping from linear attenuation to photo-electric and compton cross-sections, Φ_e and Θ_e the corresponding energy dependencies at energy e, and N_E the number of used discrete energies. The effective spectral contribution b_e is combined from:

$$b_e = s I_e D_e \tag{10}$$

where s is an overall scaling factor, I_e the X-Ray source spectrum and D_e the detector spectral sensitivity. b_e can be parameterized depending on the unknown radiometric components, and directly optimized by the framework presented above.

III. Results

A. System Setup

Our experimental setup consists of a medical X-Ray source and flat panel detector mounted in steady position, with a distance of X-Ray focal spot and detector center of about $55cm$. The detector has a direct deposit CsI scintillator, $N_L = 0.7$ Mega pixel, and a pixel size of $0.1mm$. A cheap turntable which does not run very smoothly is moving the object to be reconstructed. This allows us to investigate the automatic computation of varying angular increments o_i.
Our reconstruction algorithm computes one OS-SIRT run with 650 X-Ray projections and $N_V = 512^3$ voxels in $\approx$ 12 seconds, using an AMD Radeon 5870 GPU. In self-calibration mode, a reconstruction completes in one second, with downscaled projections ($N_L = 170K$ pixels) and $N_V = 256^3$. Depending on the number of open parameters, a full optimization terminates within one to a few minutes. We obtain similar computation times on a NVIDIA GeForce GTX 580 board.

B. Geometric Calibration on Ground Truth Phantom

In order to validate our self-calibration technique, we acquired a sequence of a cylindrical phantom with eight steel balls to compute the exact projection geometry. In a first step we automatically extract the steel balls from the projection images by using an isocontour-tracing algorithm with the isovalue chosen as the mean between the background and the steel ball intensities in the projection images. Subsequently a circle was fitted to the extracted isocontours using a least-squares minimization. The recovered center-points for each sphere over the sequence together with the approximate 3D position of the spheres are then used in a bundle adjustement step [5] to optimize both the projection geometry parameters as defined in section II-C and the position of the steel balls. The starting point for the parameters is chosen quite roughly with all parameters set to zero except the source-detector distance which was set to 500 mm. After convergence we kept the internal parameters $\mathbf{K}$ fixed, and optimized the angle offset o_i for each frame which describes the deviation from the expected rotation angle of the device. Afterwards we repeated these two optimization steps on the results. As expected, no significant changes occured in the parameters after the first run, indicating that the optimization successfully converged. In total, the bundle adjustment step required 9 iterations and resulted in an average reprojection error of 0.54 pixels. The global and frame-specific parameters are henceforth used as Ground Truth data. The reprojection error using the parameters of the self-calibrating reconstruction is 1.68 pixels.

The first two columns of table I show the parameters obtained using both the Ground Truth calibration, and our proposed reconstruction-based optimization scheme. The recovered values are very similar except for the detector offset in x-direction and the detector skew. However, it seems that these two parameters are not totally orthogonal and therefore tend to increase together. Figure 1 shows the results for the angle offset o_i computed using the Ground Truth and the self-calibration method. As can be seen the shape of the curves - in particular the local extrema - is almost identical. The mean difference is 0.24, the maximum 0.79, and the standard deviation 0.18, each expressed in terms of the regular frame angular increment, which amounts to $0.55°$. There is only a slight offset in the absolute value. This shows that the two methods are comparable in terms of accuracy, when executed on the same phantom image data.

	Ground Truth	Self-Cal. Phantom	Self-Cal. Jaw
Source-detector distance	546.7mm	549.9mm	543.4mm
Detector tilt	5.97°	5.92°	6.15°
Detector offset x	12.9mm	1.31mm	3.62mm
Detector offset y	0.42mm	0.58mm	0.75mm
Detector shear	19.5mm	1.26mm	3.61mm

TABLE I
COMPARISON OF THE RESULTING PROJECTION GEOMETRY PARAMETERS

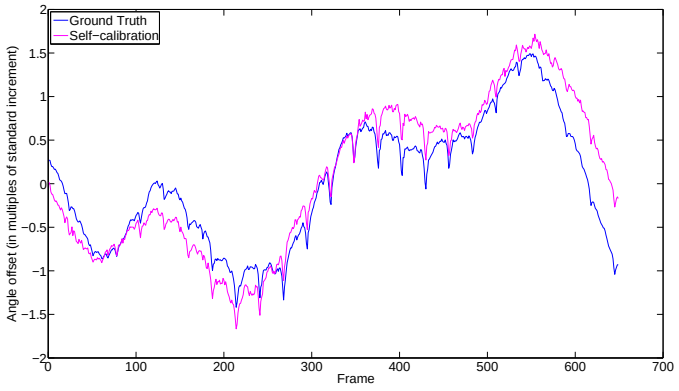

Fig. 1. Angle offset comparison between Ground Truth and self-calibration.

C. Geometric Calibration on Real Anatomy

An ex-vivo porcine jaw with dental implants was used as anatomical test data set. To test the convergence of our self-calibration, the source-detector distance was set to 500 mm, all other values (last four rows in table I) to zero as initial estimate. The self-calibrating reconstruction converged with visually excellent image quality, the resulting parameters are depicted in the last column of table I. Apart from the connected detector scale & shear, the parameters agree quite well with the Ground Truth phantom. Note that a deviation of source-detector distance of 3.3 mm corresponds to a fan-beam angle error of only $\approx 0.06°$. Figure 2 shows a reconstruction using the initial and final parameters (in the latter, the individual frame angles are optimized as well).
The angle increment optimization result on this data is shown in figure 2(c), executed a second time after completing a reconstruction with the updated angles. While the turntable

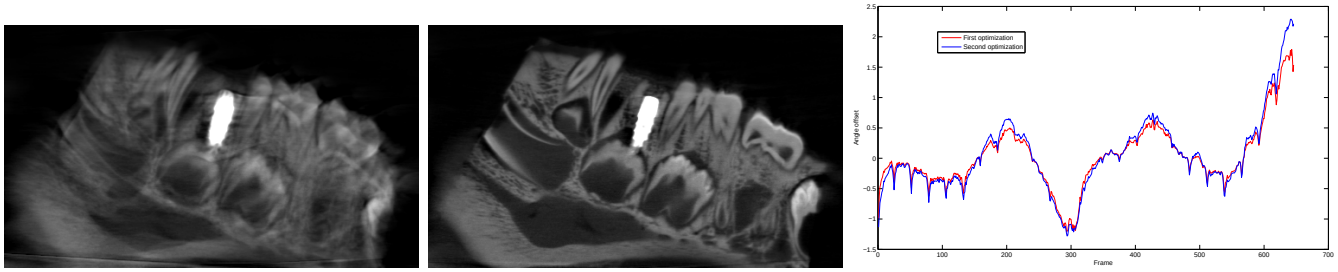

(a) initial estimate (b) geometry & angles optimized (c) angle offsets

Fig. 2. Sagittal slices from reconstruction and angle plot, illustrating geometry optimization on porcine jaw.

motion is not reproducible and can therefore not be compared to figure 1, it shows the same characteristic extrema. The second optimization causes slightly more pronounced peaks, indicating that the system converges well.

D. Radiometric Calibration on QA Phantom

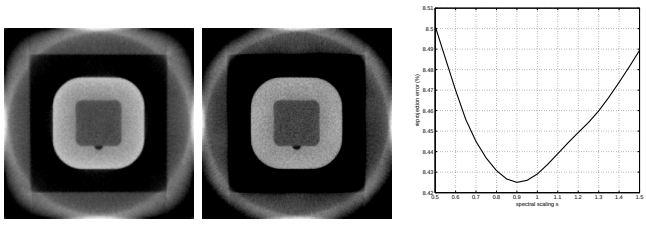

(a) $s = 0.5$ (b) $s = 0.9$ (c) residual error wrt. s

Fig. 3. Polychromatic reconstruction on phantom evaluated against s

The optimization of the radiometric scaling parameter s in equation 10 was evaluated on a Quart DVT_AP quality assurance (QA) phantom (Quart GmbH, Zorneding, Germany), running the polychromatic reconstruction algorithm outlined in section II-D. As can be seen in figure 3, the reprojection error E_k has a clear minimum at $s \approx 0.9$. The corresponding reconstruction slice has sharper edges and constant intensity across the bright ring, while a beam hardening effect is visible on the reconstruction with $s = 0.5$.

IV. Discussion

We have developed a method that allows for self-calibration of global geometric, local per-frame, and radiometric parameters on the individual scans of a cone-beam CT system, without the need for additional calibration phantom acquisitions. It is based on optimizing over the residual error of a rapid OS-SIRT algorithm, a single execution of which takes one second on recent GPU hardware.

We demonstrated the potential of this method by recovering the global geometric parameters as well as individual angle increments of a steel beads phantom and ex-vivo porcine anatomy, comparing them against a numerical computation based on the segmented bead locations. Last but not least, we could successfully eliminate beam hardening artifacts by optimizing an unknown parameter of a simplified spectral model.

The main limitation of our method stems from the fact that it is essentially a local optimization whose results depend to some extent on the underlying image data. Future work comprises to systematically evaluate the optimal parameterization, parameter dependencies, optimization capture range, as well as the influence of significantly different anatomy being imaged. So far our studies revealed that slow variations of calibration parameters which would typically occur in practice, can reliably be recovered.

Even though it is subject to continued development, we believe this method will eventually push the limit regarding image quality on affordable CT devices with mechanical imperfections. It could also enable new devices to recover physical parameters like X-ray source spectra and detector spectral sensitivity right in the software, which are otherwise difficult to obtain. This in turn can yield advances in the field of quantitative CT for small devices. A clinical 3D reconstruction today is available in the matter of seconds for presentation to the doctors, using valid calibration parameters. Future systems could use the idle time between scans, or overnight downtime, to review the consistency of, and iteratively recalibrate, all prior clinical scans. Slowly changing parameters caused by mechanical wear, burn-in of the X-Ray tube, or changing detector properties, can therefore be automatically updated. This could make regular maintenance and calibration of such systems a thing of the past, further cutting on cost-of-ownership.

References

[1] M. Mitschke and N. Navab, "Recovering the X-ray projection geometry for three-dimensional tomographic reconstruction with additional sensors: Attached camera versus external navigation system," *Medical Image Analysis*, vol. 7, pp. 65–78, 2003.

[2] N. Navab, A. Bani-Hashemi, M. Mitschke, D. W. Holdsworth, R. Fahrig, A. J. Fox, and R. Graumann, "Dynamic geometrical calibration for 3-D cerebral angiography," in *SPIE Medical Imaging conference*, Feb. 1996.

[3] Y. Kyriakou, R. Lapp, L. Hillebrand, D. Ertel, and W. Kalender, "Simultaneous misalignment correction for approximate circular cone-beam computed tomography," *Physics in Medicine and Biology*, vol. 53, pp. 6267–6289, 2008.

[4] F. Xu, W. Xu, M. Jones, B. Keszthelyi, J. Sedat, D. Agard, and K. Mueller, "On the efficiency of iterative ordered subset reconstruction algorithms for acceleration on GPUs," *Computer Methods and Programs in Biomedicine*, vol. 98, pp. 261–270, Jun. 2010.

[5] R. I. Hartley and A. Zisserman, *Multiple View Geometry in Computer Vision*, 2nd ed. Cambridge University Press, 2004.

[6] B. D. Man, J. Nuyts, P. Dupont, G. Marchal, and P. Suetens, "An iterative maximum-likelihood polychromatic algorithm for CT," *IEEE Transactions on Medical Imaging*, vol. 20, pp. 999–1008, Oct. 2001.